Protein phosphatase 2A activation as a therapeutic strategy for managing MYC-driven cancers

Received for publication, October 10, 2019, and in revised form, December 4, 2019 Published, Papers in Press, December 10, 2019, DOI 10.1074/jbc.RA119.011443

Caroline C. Farrington[‡], Eric Yuan[§], Sahar Mazhar[¶], Sudeh Izadmehr[‖1], Lauren Hurst[**], Brittany L. Allen-Petersen[‡‡], Mahnaz Janghorban[‡‡], Eric Chung[§], Grace Wolczanski[**], Matthew Galsky[‖], Rosalie Sears[‡‡], Jaya Sangodkar[**], and Goutham Narla[2]**

*From the Departments of [‡]Pharmacology and [¶]Pathology and the [§]Case Comprehensive Cancer Center, Case Western Reserve University, Cleveland, Ohio 44106, the [‖]Department of Medicine, Division of Hematology and Medical Oncology, Tisch Cancer Institute, Icahn School of Medicine at Mount Sinai, New York, New York 10029, the [**]Division of Genetic Medicine, Department of Internal Medicine, University of Michigan, Ann Arbor, Michigan 48105, and the [‡‡]*Department of Molecular and Medical Genetics, Oregon Health and Sciences University, Portland, Oregon 97239

Edited by Alex Toker

The tumor suppressor protein phosphatase 2A (PP2A) is a serine/threonine phosphatase whose activity is inhibited in most human cancers. One of the best-characterized PP2A substrates is MYC proto-oncogene basic helix–loop–helix transcription factor (MYC), whose overexpression is commonly associated with aggressive forms of this disease. PP2A directly dephosphorylates MYC, resulting in its degradation. To explore the therapeutic potential of direct PP2A activation in a diverse set of MYC-driven cancers, here we used biochemical assays, recombinant cell lines, gene expression analyses, and immunohistochemistry to evaluate a series of first-in-class small-molecule activators of PP2A (SMAPs) in Burkitt lymphoma, KRAS-driven non–small cell lung cancer, and triple-negative breast cancer. In all tested models of MYC-driven cancer, the SMAP treatment rapidly and persistently inhibited MYC expression through proteasome-mediated degradation, inhibition of MYC transcriptional activity, decreased cancer cell proliferation, and tumor growth inhibition. Importantly, we generated a series of cell lines expressing PP2A-dependent phosphodegron variants of MYC and demonstrated that the antitumorigenic activity of SMAPs depends on MYC degradation. Collectively, the findings presented here indicate a pharmacologically tractable approach to drive MYC degradation by using SMAPs for the management of a broad range of MYC-driven cancers.

The oncogene *MYC* is frequently amplified or overexpressed in many cancer types, independent of histological subtype, and increased MYC expression is correlated with both more-aggressive disease and resistance to standard-of-care treatments (1–5). Moreover, studies have demonstrated that c-MYC (MYC) drives transformation, tumor growth, and metastasis (5–7). As a result, MYC is a well-validated and desirable drug target. However, despite its well-validated role as a driver oncogene, MYC has gained a reputation for being "undruggable" because of its lack of a defined and structured ligand-binding site, nuclear localization, and its complex regulation at the transcriptional and post-translational levels (8). In attempts to target MYC, researchers have developed alternative approaches to antagonize MYC activity including the development of Omomyc, a dominant negative form of MYC (9–14), and bromodomain inhibitors that have been well-characterized to inhibit the transcription of *MYC* and MYC target genes through their inhibition of superenhancer elements (15–20). Other direct and indirect approaches have also been developed that have been very thoroughly reviewed in the literature (8, 21, 22). Overall, these efforts highlight the central dependence of cancers on MYC signaling and demonstrate that targeting MYC function could represent an attractive approach for the treatment of a broad range of cancers. Here, we present a therapeutic strategy that promotes the rapid degradation of MYC protein, resulting in tumor inhibition and robust inhibition of MYC transcriptional activity.

Protein phosphatase 2A (PP2A)[3] is a well-characterized tumor suppressor, whose inactivation is critical for cellular

This work was supported by NCI, National Institutes of Health Grant R01CA181654 (to G. N. and M. G.). This work was also supported by the Athymic Animal and Preclinical Therapeutics and Cytometry, Imaging Microscopy Shared Resources of the Case Comprehensive Cancer Center Grant P30CA043703, and Icahn School of Medicine at Mount Sinai Microscopy Core Grant P30CA196521. The Icahn School of Medicine at Mount Sinai has filed patents covering composition of matter on the small molecules disclosed herein for the treatment of human cancer and other diseases (International Application Numbers: PCT/US15/19770, PCT/US15/19764; and US Patent: US 9,540,358 B2). Mount Sinai is actively seeking commercial partners for the further development of the technology. G. N. has a financial interest in the commercialization of the technology. The content is solely the responsibility of the authors and does not necessarily represent the official views of the National Institutes of Health.

This article contains Tables S1–S3 and Figs. S1–S9.

[1] Supported by the Loan Repayment Program of the National Institutes of Health/National Center for Advancing Translational Sciences.

[2] To whom correspondence should be addressed: Division of Genetic Medicine, Dept. of Internal Medicine, University of Michigan, Ann Arbor, MI 48105. Tel.: 734-615-2411; Fax: 734-647-9647; E-mail: gnarla@med.umich.edu.

[3] The abbreviations used are: PP2A, protein phosphatase 2A; SMAP, small-molecule activators of PP2A; TUNEL, terminal deoxynucleotidyltransferase-mediated dUTP nick end labeling; GEMM, genetically engineered mouse model; NSCLC, non–small cell lung cancer; IHC, immunohistochemistry; TNBC, triple-negative breast cancer; AR, androgen receptor; DMEM, Dulbecco's modified Eagle's medium; MTT, 3-(4,5-dimethylthiazol-2-yl)-2,5-diphenyltetrazolium bromide; DMA, *N*,*N*-dimethylacetamide; H&E, hematoxylin and eosin; EGFP, enhanced green fluorescence protein; PI, propidium Iodide.

transformation and whose activity is functionally inhibited by a diverse range of mechanisms in a wide variety of cancers (23–29). Its tumor suppressive activity is exerted through its ability to dephosphorylate a number of substrates involved in the regulation of cell growth and survival, including the MYC protein (30–33). MYC activity is dynamically regulated through a series of phosphorylation and dephosphorylation events that allow for the rapid induction of MYC-dependent transcription. PP2A-mediated dephosphorylation of MYC at serine 62 leads to its degradation through the ubiquitin–proteasome pathway and provides essential negative regulation of this potent oncoprotein. In cancer, however, MYC is often aberrantly phosphorylated at Ser^{62}, leading to its stabilization and increased activity (7, 32, 33). As such, we hypothesized that if the tumor suppressive activity of PP2A could be re-engaged/re-activated in cancer cells, this may prove to be a viable approach to the therapeutic targeting of MYC in cancer models.

Although PP2A activation as a strategy to target MYC has been proposed and demonstrated previously, these studies relied on indirect methods of activating PP2A (8, 34–44). Here, we utilized a direct approach of targeting PP2A using small molecule activators of PP2A, or SMAPs. These molecules have been well-characterized for their target specificity, toxicology, and antitumorigenic properties *in vivo* (45–49). Specifically, binding studies have demonstrated that these molecules bind to the A subunit scaffold of PP2A, and biological assays have demonstrated that the ability to bind to PP2A is necessary to achieve their antitumorigenic effects. The target specificity of these small molecules has been extensively studied and reported on previously (46–48). Moreover, no visible toxicities have emerged in previous *in vivo* studies as measured by gross behavioral observations, a lack of weight loss, and no perturbations to serum chemistries or complete blood counts in chronically treated mice (45–49). We hypothesized that given the negative regulation of MYC by PP2A, SMAP-mediated activation of PP2A may represent a unique therapeutic strategy for targeting MYC signaling in cancer cells.

Recent publications have used SMAPs to demonstrate PP2A-mediated changes to MYC in specific tumor types (46, 50). However, a comprehensive attempt to profile the ability of PP2A reactivation to treat MYC-driven cancers has yet to be studied. Here, we show that direct activation of PP2A by SMAPs *in vivo* results in tumor growth inhibition across numerous models of MYC-driven cancers and extends previous findings beyond just subcutaneous xenotransplanted models of cancer. Additionally, this current work demonstrates that SMAPs inhibit MYC signaling regardless of the mechanism by which MYC drives any given cancer. We selected models based on both prevalence and mechanism by which MYC activity is increased—specifically, Burkitt's lymphoma (MYC genetic amplification), KRAS mutant non–small cell lung cancer (post-translational stabilization of MYC), and triple-negative breast cancer (MYC overexpression). Furthermore, we utilized three distinct SMAP molecules, SMAP1, SMAP2, and SMAP3 (Fig. S1) (48) to further validate our hypothesis that PP2A activation may drive tumor growth inhibition in MYC-driven cancers. These molecules are structurally similar PP2A-specific activators whose difference lays primarily in their relative potency and pharmaceutic properties (44, 46), and the use of multiple independent small molecule PP2A activators rules out potential off-target effects of any individual molecule, providing further evidence that the observed biology is PP2A-dependent. In addition to the tumor growth inhibition noted in all models, molecular analysis of treated tumors revealed a significant decrease in total MYC protein expression and a corresponding decrease in MYC signaling, confirming decreased MYC activity in both cellular and *in vivo* models. Furthermore, we demonstrate that the decrease in MYC protein levels results from changes in MYC protein stability as a result of proteasome-mediated protein degradation upon PP2A-mediated dephosphorylation. In support of this finding, tumors expressing mutations in the phosphodegron of MYC were no longer responsive to SMAP treatment. Collectively, our data show that direct activation of PP2A is a promising therapeutic strategy for the treatment of MYC-driven cancers.

Results

SMAPs inhibit tumor growth in c-MYC-driven Burkitt's lymphoma

Burkitt's lymphoma is a disease that has been shown to almost universally be driven by MYC as result of one of three translocations that drives high *MYC* expression and activity (51). As a result of this driver event, there is little genetic heterogeneity in this model, making it an ideal system to study the therapeutic potential of PP2A reactivation for the treatment of MYC-driven cancers. Therefore, to investigate whether direct small molecule–mediated activation of PP2A inhibits tumor growth in MYC-driven cancers, we treated a xenograft model of Burkitt's lymphoma with SMAPs and monitored tumor growth. To establish efficacy in this model, we used the Burkitt's lymphoma cell line Daudi in a subcutaneous xenograft model (Fig. 1*A*). Mice were treated with 15 mg/kg SMAP1 twice a day per previously published, and unpublished data using a range of SMAPs from 0.1 to 50 mg/kg dosed either twice a day or once a day demonstrated that doses between 5 and 15 mg/kg twice a day resulted in optimal tumor growth inhibition (46–50). Treatment with higher SMAP concentrations, although well-tolerated in mice, did not result in significant difference in response; thus, we have used 15 mg/kg in the majority of studies presented here. In this model, SMAPs inhibited tumor growth by ~65% (Fig. 1, *A* and *B*). As has been shown previously (47, 48), SMAP1 treatment was well-tolerated with no visible toxicities or changes in body weight noted over the entire treatment course (Fig. S2*A*). At the end of the study, control and SMAP-treated tumors were analyzed for phosphorylation of MYC at serine 62 as well as total MYC expression and apoptosis by immunoblot and TUNEL staining, respectively. Phosphorylated MYC and total MYC protein expression were determined to be significantly decreased in SMAP-treated tumors compared with control tumors (Fig. 1, *C* and *D*). Additionally, TUNEL staining analysis revealed a significant increase in apoptosis in the SMAP-treated tumors compared with control tumors (Fig. 1, *E* and *F*). Taken together, these data established the efficacy of SMAP treatment in the Burkitt's lymphoma Daudi model, suggesting that this is a viable approach for tar-

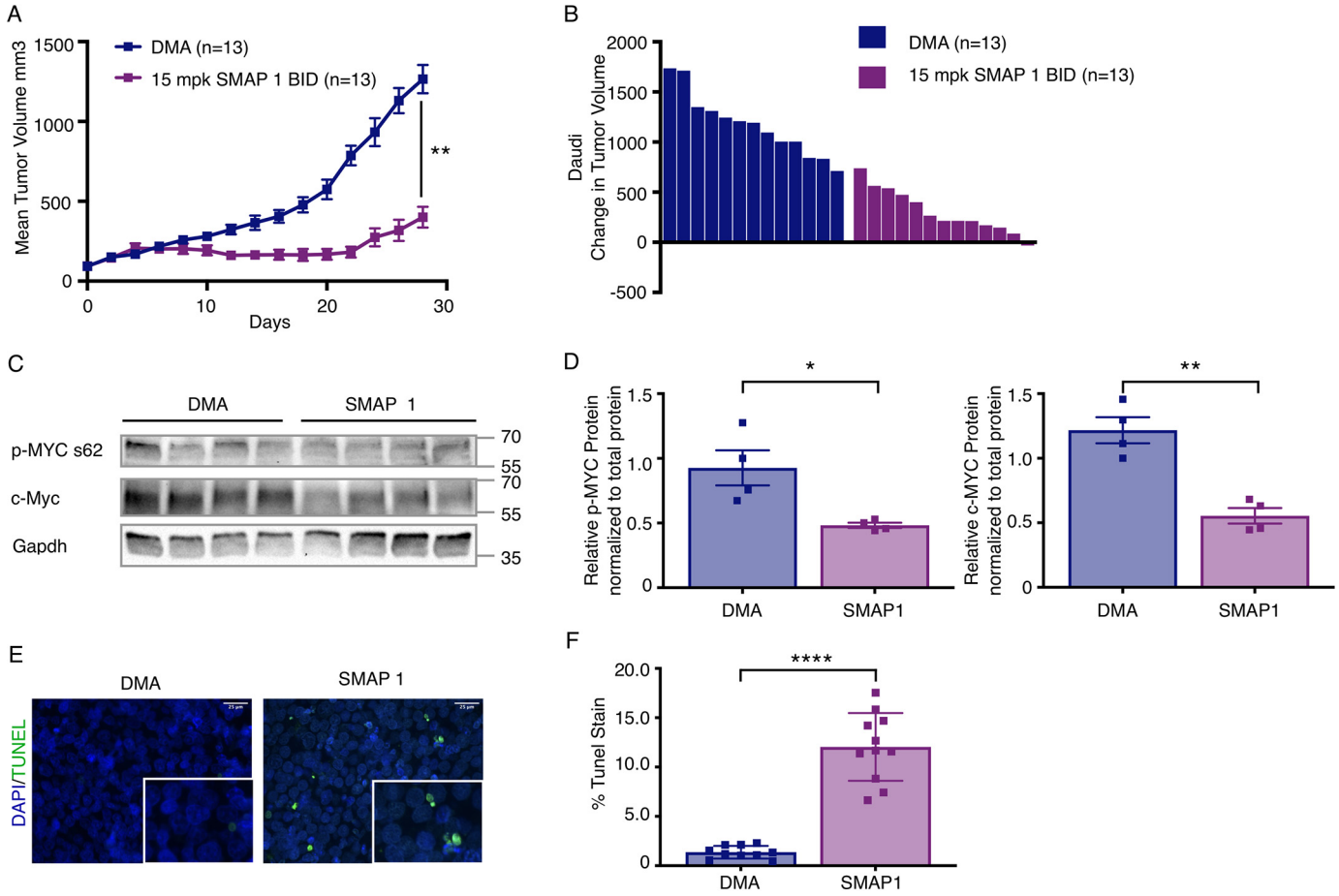

Figure 1. SMAPs inhibit tumor growth and decrease c-MYC expression in a model of Burkitt's lymphoma. *A*, tumor growth in a xenograft model of Burkitt's lymphoma with the Daudi cell line treated with DMA (control) or 15 mg/kg SMAP1 by oral gavage twice a day. *B*, change in individual tumor volume at end of study. *C*, Western blotting for c-MYC expression from tumor lysates. *D*, quantification of p-MYC (Ser^{62}) and MYC expression normalized to total protein. Stain-free images used for normalization are included in Fig. S3*A*. *E*, representative images of TUNEL staining in tumors treated with DMA or SMAPs. *F*, quantification of TUNEL. Respective quantifications are represented as means ± S.E. (*A*) or means ± S.D. (*D* and *E*). **, $p < 0.01$; ****, $p < 0.0001$. *BID*, twice per day; *DAPI*, 4′,6′-diamino-2-phenylindole.

geting MYC and driving an antitumorigenic response as a result.

SMAPs decrease tumor burden and c-MYC expression in a KRAS model of non–small cell lung cancer

Next, we extended our studies to a genetically engineered mouse model (GEMM) of KRAS driven non–small cell lung cancer (NSCLC), $KRAS^{LA2}$ (52). It has been established that MYC and KRAS cooperate to drive tumorigenesis and that KRAS mutant tumors can be dependent on MYC for their survival (53–55). MYC has been shown to be overexpressed broadly in up to 70% of NSCLC, and MYC overexpression is associated with a poor prognosis (56–58). In KRAS mutant NSCLC specifically, MYC protein is further stabilized by a KRAS downstream kinase, extracellular signal-regulated kinase, via phosphorylation at serine 62, the same site previously described to be dephosphorylated by PP2A (12, 32, 59–61). Through this mechanism, MYC is a critical effector of KRAS-mediated activity and could represent a potential drug target for the treatment of KRAS-driven cancers (12, 59). We therefore hypothesized that PP2A reactivation could represent a novel strategy for the treatment of KRAS mutant lung cancer through its negative regulation of MYC. We began by determining the expression of MYC in the tumors from the $KRAS^{LA2}$ (52) GEMM of lung cancer *versus* WT mice using immunohistochemistry (IHC) (Fig. 2*A*). Importantly, there was a significant increase in MYC expression in the KRAS mutant mice compared with control mice, supporting the findings that MYC protein is stabilized by KRAS-dependent signaling. We next treated the $KRAS^{LA2}$ GEMM of lung cancer with SMAP2 for 28 days. At the end of the study, the mice were sacrificed, and the lungs were removed for downstream molecular and histological analysis. Consistent with previous results, overall tumor volume was significantly decreased in SMAP2-treated mice compared with control, consistent with a marked reduction in lung cancer nodules as measured by histological quantitation (Fig. 2, *B–D*). The observed reduction in tumor growth was associated with an increase in apoptotic signaling in the tumor nodules of SMAP2-treated mice compared with control as measured by TUNEL staining (Fig. 2*B* and Fig. S4*A*) and a decrease in MYC expression (Fig. 2*B*). These data provide further support to our hypothesis that PP2A activators may have robust antitumor activity through their ability to regulate MYC expression and signaling.

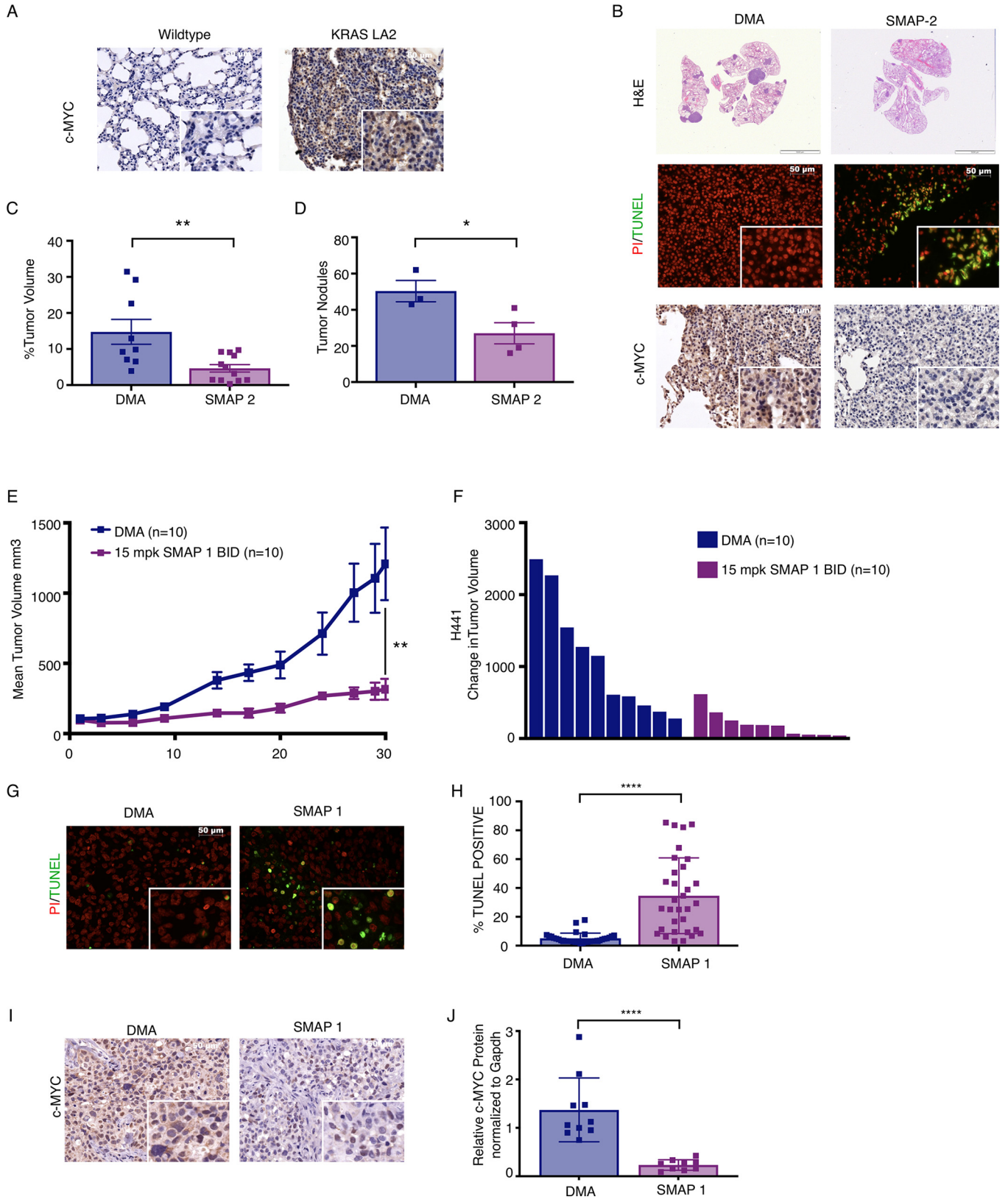

Figure 2. SMAPs inhibit tumor growth and decrease c-MYC expression in KRAS driven NSCLC. *A*, immunohistochemistry for c-MYC expression in lung tissue of WT and KRAS LA2 GEMM of NSCLC. *B*, H&E of lungs, TUNEL staining, and immunohistochemistry for c-MYC in lungs from KRASLA2 mice treated with vehicle control (DMA) or SMAP2. *C*, percentage of tumor volume in lungs of KRASLA2 mice treated with DMA or SMAP2. *D*, number of tumor nodules in lungs. *E*, tumor growth in a H441 xenograft model of NSCLC treated with DMA or SMAP1. *F*, change in individual tumor volume at end of study. *G*, representative images of tumors from H441 xenograft stained for propidium iodide (PI) and TUNEL. *H*, quantification of TUNEL. *I*, representative images of c-MYC expression in H441 tumors by IHC. *J*, quantification of c-MYC expression from tumor lysates assessed by Western blotting in Fig. S3*A*. Respective quantifications are represented as means ± S.D. *, $p < 0.05$; **, $p < 0.01$; ****, $p < 0.0001$. *BID*, twice per day; *mpk*, mg/kg.

In addition to the $KRAS^{LA2}$ model of non–small cell lung cancer, we also assessed response to SMAP treatment in a subcutaneous xenograft model of KRAS-driven lung cancer using the H441 cell line, which harbors a KRAS G12V mutation. We have previously shown that SMAPs have activity in H441 *in vitro*. (48) To determine whether SMAP treatment inhibited H441 tumor growth *in vivo*, we performed a subcutaneous xenograft and treated with SMAP1. We found that SMAP1 significantly inhibited tumor growth by ~76% (Fig. 2, *E* and *F*). Additionally, tumors treated with SMAP1 showed a significant increase in TUNEL positivity indicative of apoptosis when compared with control tumors (Fig. 2, *G* and *H*). Finally, we analyzed MYC expression by IHC, and as hypothesized, greater MYC expression was seen in tumors from the control group, supportive of the coupled relationship between KRAS and MYC activation (Fig. 2*I*). Consistent with our results with the $KRAS^{LA2}$ GEMM, tumors treated with SMAP1 had lower $Ser(P)^{62}$ and total MYC expression as determined by both IHC and Western blotting (Fig. 2, *I* and *J*, and Fig. S4, *B–D*). Combined, these findings suggest that the therapeutic efficacy of small molecule–mediated reactivation of PP2A may be a result of coordinate down-regulation of both MYC and KRAS signaling.

SMAPs inhibit tumor growth in c-MYC expressing xenograft models of TNBC

To extend the translational impact of our findings, we investigated the potential of SMAPs to inhibit tumor growth in xenograft models of triple-negative breast cancer (TNBC). TNBC is a breast cancer subtype that is notoriously aggressive and less responsive to current standard-of-care treatments. *MYC* has been well-described to be commonly overexpressed and functionally active in claudin-low and basal-like TNBC (57). Moreover, high *MYC* expression in these subtypes is associated with poor response to current standard-of-care treatments (62). It has been shown that the high expression of MYC contributes to a state of MYC oncogene addiction in these cancers and as such has been well-described as a potential drug target for the treatment of TNBC (34, 57, 63–65). In support of this, it has previously been shown that direct or indirect inhibition of MYC inhibits disease progression in both *in vitro* and *in vivo* models of the disease (16, 34, 64, 66).

First, we performed *in vitro* studies to test SMAP response in a series of TNBC cell lines, MDA-MB-231, MDA-MB-453, BT549, and HCC1937. All lines were sensitive to SMAP treatment as demonstrated by dose-dependent decreases in cell viability and reduced colony formation in a mammosphere assay (Fig. S5, *A–D*). Moreover, in the mammosphere assay, HCC1143 appears to be more sensitive to SMAPs than to the standard of care for TNBC, paclitaxel, as well as the MEK inhibitor AZD6244, which has previously been proposed as a targeted therapy approach for TNBC (67, 68).

To extend these findings to disease relevant *in vivo* models, we tested SMAP efficacy in a series of TNBC xenograft models. We selected three TNBC cell lines, previously characterized for their high *MYC* expression and MYC dependence for efficacy testing with our small molecule PP2A activator series. The MDA-MB-231 cell line is a claudin-low TNBC cell line that harbors a KRAS mutation that is proposed to contribute to MYC stability much like the lung cancer models described above (57). The SUM149PT line is a basal-like TNBC cell line that demonstrates MYC dependence (63). Finally, we used the MDA-MB-453, a TNBC cell line that expresses the androgen receptor (AR) and high levels of the MYC protein. Importantly, much like what has been shown in prostate cancer, there is a strong relationship in breast cancer between MYC and AR pathway activation and increased tumorigenesis and drug resistance (69, 70). Treatment with SMAP1 induced tumor growth inhibition of 46% in the MDA-MB-231 model (Fig. 3, *A* and *B*), 68% in the MDA-MB-453 model (Fig. 3, *E* and *F*), and 69.7% in the SUM149PT model (Fig. 3, *G* and *H*). Again, no significant weight loss or visible toxicities were identified in the treated mice, consistent with previous *in vivo* studies performed (Fig. S2, *B* and *C*). In the MDA-MB-231 model, the antitumor effects of SMAP1 was comparable with that of paclitaxel (Fig. 3, *A* and *B*), and SMAP-treated tumors demonstrated decreased phosphorylation of MYC at serine 62, as well as a decrease in total MYC protein expression (Fig. 3, *C* and *D*). Importantly, in the MDA-MB-453 model, the majority of tumors regressed upon treatment with SMAPs (Fig. 3*D*). As a result of their small size or lack of remaining tumor, MYC expression could not be assessed in SMAP-treated tumors from the MDA-MB-453 or SUM149PT models. Collectively, our findings demonstrate that SMAP treatment inhibits tumor growth in multiple models of MYC-expressing TNBC.

SMAP treatment results in proteasome-mediated MYC degradation

To determine the mechanism by which PP2A activation alters MYC expression, we treated Daudi cells with SMAPs and analyzed MYC stability and function. Upon SMAP treatment, both phosphorylated MYC (s62) and total MYC protein expression rapidly decreased, with a greater than 50% loss seen within 2 h and minimal protein remaining by 4 h (Fig. 4, *A–C*). To determine whether these changes were occurring post-transcriptionally, we analyzed the mRNA levels of *MYC* after treatment with SMAPs and found no significant change (Fig. S6*A*), indicating that the decrease in *MYC* expression resulted from post-transcriptional mechanisms of regulation. To determine the generalizability of these findings, we assessed MYC protein expression upon PP2A activation in two of the TNBC cell lines used *in vivo*, MDA-MB-453 and MDA-MB-231. Consistent with the results in the Daudi cell line, MYC protein expression decreased within 3 h (Fig. S6, *B* and *C*). Additionally, we assessed MYC $t_{½}$ in the MDA-MB_231 cell line in the presence and absence of SMAPs using cycloheximide and found that SMAPs shortened MYC $t_{½}$ by nearly 50% from 35 to 18 min (Fig. 4, *D–F*).

Multiple publications have demonstrated that MYC stability is regulated by ubiquitination through several E3 ligases, including FBXW7. Recognition of MYC by FBXW7 is directed by PP2A-mediated Ser^{62} dephosphorylation, triggering MYC degradation by the proteasome (7, 32, 33, 71). To determine whether the SMAP-mediated decrease in MYC protein expression was proteasome-mediated, we treated cells with SMAP1 in the presence of the proteasome inhibitor MG132. Daudi cells

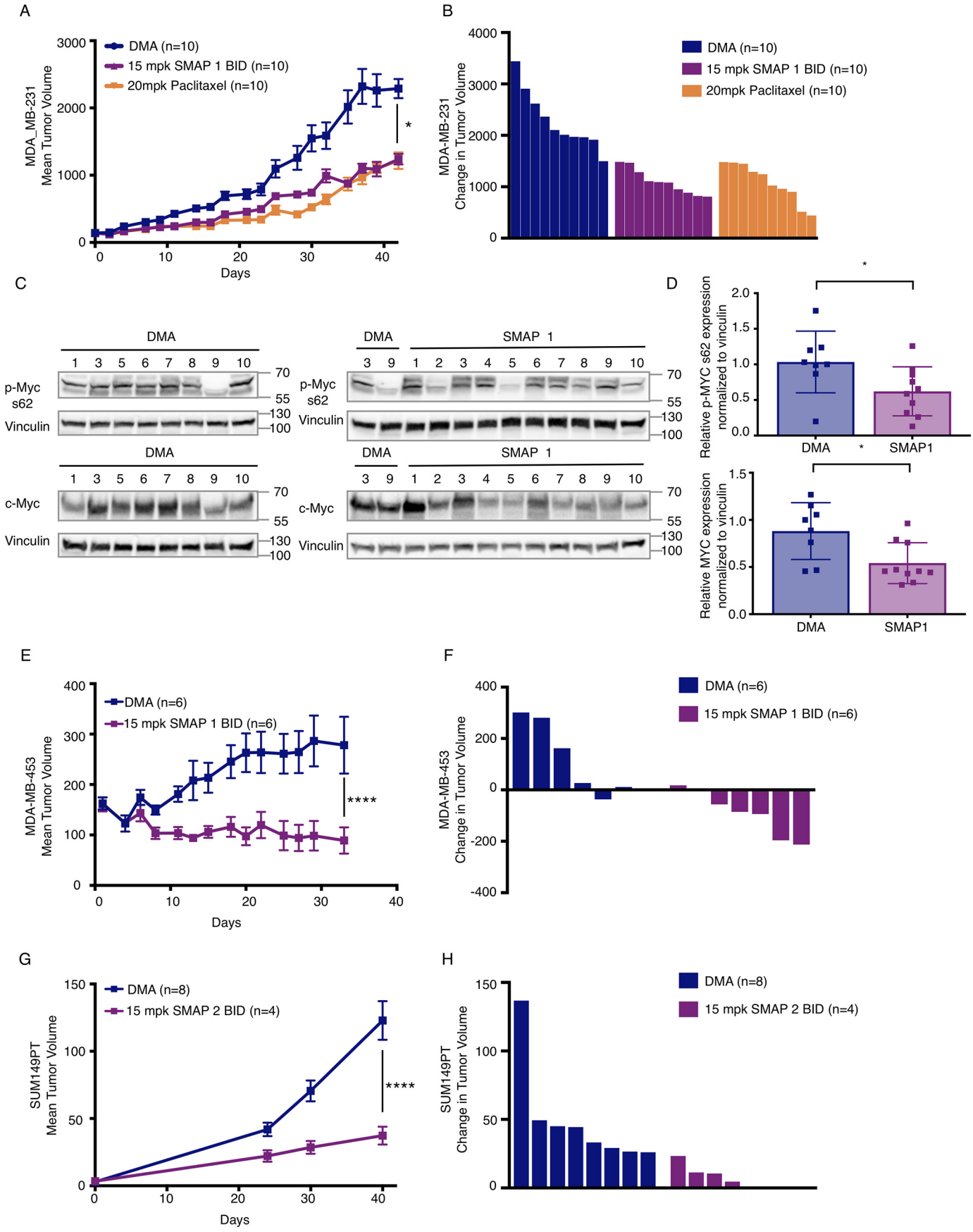
A
MDA_MB-231
Mean Tumor Volume
DMA (n=10)
15 mpk SMAP 1 BID (n=10)
20mpk Paclitaxel (n=10)
Days
B
MDA-MB-231
Change in Tumor Volume
C
DMA
SMAP 1
p-Myc s62
c-Myc
Vinculin
D
Relative p-MYC s62 expression normalized to vinculin
Relative MYC expression normalized to vinculin
DMA
SMAP1
E
MDA-MB-453
Mean Tumor Volume
DMA (n=6)
15 mpk SMAP 1 BID (n=6)
F
MDA-MB-453
Change in Tumor Volume
G
SUM149PT
Mean Tumor Volume
DMA (n=8)
15 mpk SMAP 2 BID (n=4)
H
SUM149PT
Change in Tumor Volume

were pretreated for 2 h with DMSO or MG132 and then treated with 20 μM of SMAP or DMSO for 2 h. Consistent with previous findings, total MYC expression decreased in the SMAP-treated cells (Fig. 4, *G* and *H*). However, in cells that were pretreated with MG132, these changes were significantly abrogated, indicating that the decrease in MYC expression in response to SMAP1 resulted from proteasome-mediated degradation of the protein (Fig. 4, *G* and *H*).

In summary, we show that the decrease in MYC protein expression upon PP2A activation occurs post-translationally and that this decrease could be rescued through inhibition of the proteasome consistent with the established mechanism of MYC degradation upon PP2A activation. These data, combined with the established mechanism of MYC degradation, demonstrate that small molecule activation of PP2A results in the degradation of MYC by the proteasome.

SMAPs inhibit the transcription of c-MYC target genes

Based upon the observed changes in MYC protein expression, we next sought to confirm the loss of protein by determining whether its activity was changed. A panel of well-described transcriptional targets of MYC was selected from the literature (Table S1) (72, 73), and changes in their expression were assessed after SMAP treatment in the Daudi and MDA-MB-231 cell lines. In both cell lines, 21 of 23 of the MYC gene targets that are reported to be transcriptionally up-regulated by MYC were down-regulated with SMAP treatment (Daudi: Fig. 4*F* and Table S2; MDA-MB-231: Fig. S6*D* and Table S3). Conversely, two genes shown to be transcriptionally inhibited by MYC were also assessed after SMAP treatment, and of these two targets, one (CEBPA) was significantly up-regulated in both cell lines. Overall, these changes in mRNA expression of MYC target genes demonstrate a change in MYC transcriptional output upon SMAP treatment.

Mutation of the c-MYC phosphodegron abrogates SMAP-driven tumor growth inhibition

To determine whether SMAP-induced dephosphorylation and degradation of the c-MYC protein is responsible for its reported anticancer activity, we expressed a phosphomimetic version of MYC (S62D); if SMAP-mediated dephosphorylation of MYC at this defined site drives the observed anticancer activity, then these effects will be attenuated in the presence of the phosphodegron mutant MYC S62D. To test this functional dependence, we expressed EGFP as a control, wt-MYC, MYC S62D, and a T58A MYC mutant (Fig. S7, *A* and *B*), which allows for PP2A-dependent dephosphorylation at Ser^{62} but inhibits downstream degradation of MYC to occur by preventing c-MYC from being identified by its E3 ligase.

As previously demonstrated in the parental Daudi line, SMAP treatment inhibited tumor growth in the Daudi–EGFP cell line (47%), induced tumor cell apoptosis as quantitated by TUNEL staining, and drove decreased MYC expression as observed by Western blotting of tumor lysates (Fig. 5, *A–E*). This same trend was seen in the line overexpressing WT MYC, although the effect here was modestly abrogated (31% tumor growth inhibition) (Fig. S8, *A–E*). The overexpression of MYC generally promotes more aggressive tumor growth as observed by the differences in growth between this model and parental Daudi or Daudi–EGFP, and as a result this may have affected the magnitude of SMAP response. Interestingly, in both the Daudi MYC S62D xenograft and the Daudi MYC T58A xenograft, there was no tumor growth inhibition by SMAPs (Fig. 5*F* and Fig. S8*F*). Additionally, in both of these models, SMAP treatment did not result in any significant induction of apoptosis as assessed by TUNEL staining, and MYC protein expression was unchanged in these MYC mutant xenografts (Fig. 5, *G–J*, and Fig. S8, *G–J*).

When assessing MYC expression across tumor lysates from these studies, there are two bands both migrating near the molecular weight reported for MYC that were not previously seen *in vitro*. To determine whether a single or both bands should be used to quantitate MYC expression, a blot was run with representative tumor lysates from each study. Overall, it seems that both bands were overexpressed in the models with MYC overexpression (Fig. S9*A*). Thus, to quantify MYC expression in each of the *in vivo* studies presented, both bands were analyzed. Additionally, this blot demonstrates that overexpression of MYC, MYC S62D, and MYC T58A appears to have been sustained through the course of the study. In summary, these studies demonstrate that PP2A-mediated dephosphorylation of MYC is necessary for SMAP-driven tumor growth inhibition in these models and solidify the proposed mechanism of PP2A in regulating MYC Ser^{62} phosphorylation and degradation.

Discussion

This work builds on a robust body of research demonstrating that MYC is a potent oncogene and that targeting it could be an ideal therapeutic strategy in a diverse range of cancers, many of which progress rapidly on standard-of-care treatments and in general are associated with quite poor prognosis. In the original research presented here, we have demonstrated that the degradation of the MYC protein using a first-in-class series of direct small molecule PP2A activators has significant single agent preclinical activity. Moreover, this approach has the following advantages: 1) these small molecules are orally bioavailable and well-tolerated across a number of preclinical models; 2) PP2A reactivation targets MYC at the protein level, resulting in its rapid degradation, essentially acting as a MYC degrader; and 3) the specificity of these small molecules to PP2A has been extensively validated. In aggregate, this first-in-class and pharmaceutically tractable approach targets MYC degradation, leading to a significant reduction in overall cell viability and a reduction in tumor volume *in vivo*.

One advantage to targeting MYC via PP2A reactivation is that it may overcome the diversity of mechanisms by which

Figure 3. SMAPs inhibit tumor growth in models of triple-negative breast cancer. *A*, change in mean tumor volume over time in xenograft models of triple-negative breast cancer cell lines MDA-MB-231. *B*, Western blotting for phospho-MYC (serine 62) and total MYC in control and treated tumors. *C*, quantification of phospho-MYC and total MYC expression across tumors in *B*. *E* and G, expression levels all normalized to DMA tumor 3 MDA-MB-453 (*E*) and SUM149PT (*G*) treated with DMA and SMAP1 by oral gavage twice a day and in MDA-MB-231 paclitaxel once per week intraperitoneally. *B*, *D*, and *F*, individual changes in tumor volume at end of study quantified in MDA-MB-231 (*B*), MDA-MB-453 (*D*), and SUM149PT (*F*). Respective quantifications are represented as means ± S.D. *, $p < 0.05$; **, $p < 0.01$; ****, $p < 0.0001$. *BID*, twice per day; *mpk*, mg/kg.

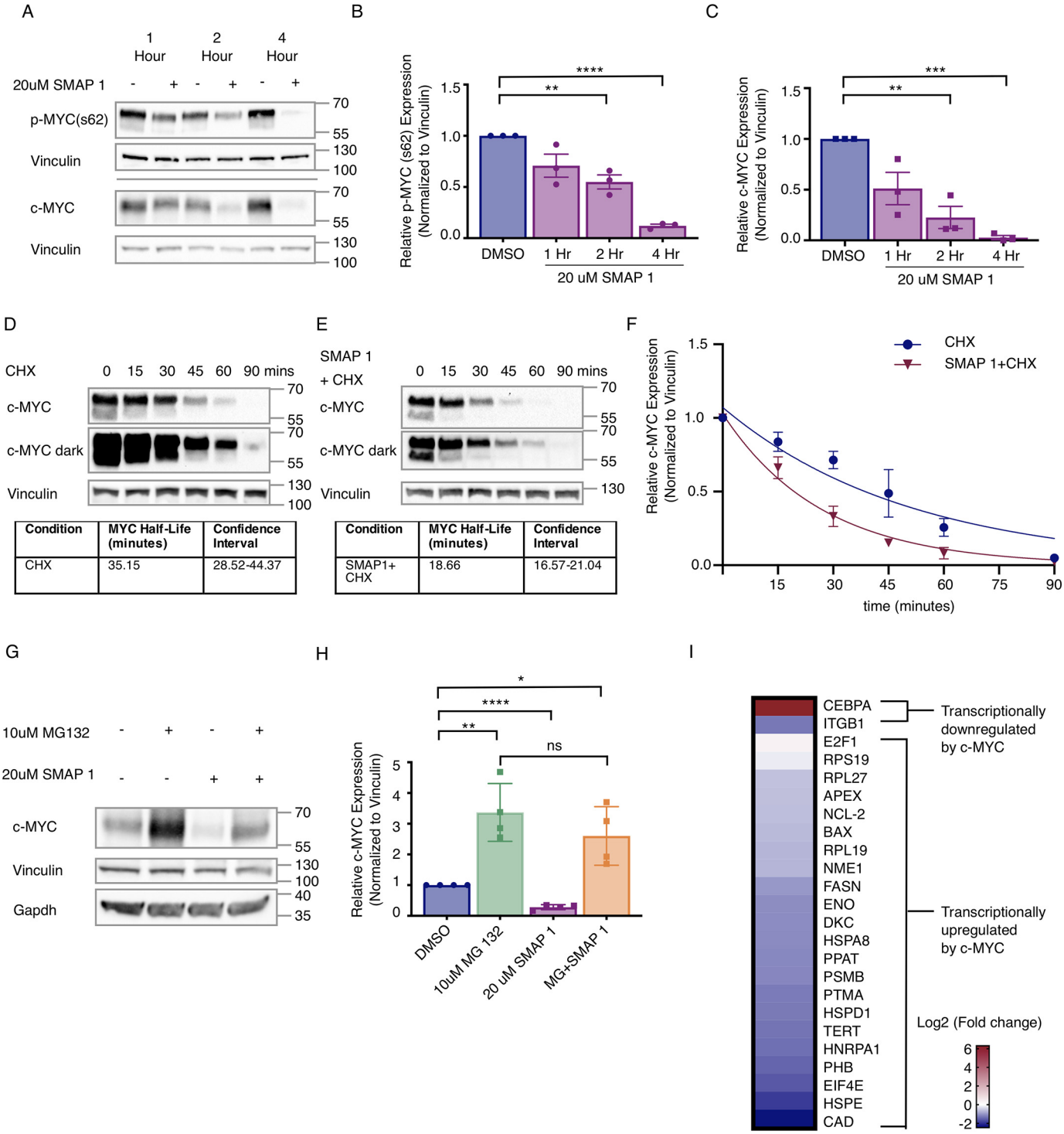

Condition	MYC Half-Life (minutes)	Confidence Interval
CHX	35.15	28.52-44.37

Condition	MYC Half-Life (minutes)	Confidence Interval
SMAP1+ CHX	18.66	16.57-21.04

Figure 4. SMAPs decrease c-MYC expression through a proteasome-mediated mechanism and induce changes to c-MYC target genes. *A*, Western blotting for Ser(P)[62] and total c-MYC in Daudi cell line after exposure to 20 μM SMAP1 over 1, 2, or 4 h. *B* and *C*, quantification of phospho-MYC (*B*) and total c-MYC (*C*) protein in $n = 3$ experiments normalized to vinculin. D, Western blotting of MDA-MB-231 cells treated with cyclohexamide (*CHX*) over time and calculation of MYC $t_{1/2}$. *E*, Western blotting for c-MYC expression in cells co-treated with SMAP1 and cyclohexamide over time and calculation of MYC $t_{1/2}$. *F*, quantification of MYC in *D* and *E* over time used for calculation of c-MYC half-life in each condition and confidence interval. *G*, Western blotting for c-MYC expression upon treatment with MG132, SMAP1, or combination. *H*, quantification of *G* for $n = 3$. *I*, changes to mRNA expression of c-MYC target genes in Daudi cell line upon treatment with 20 μM SMAP1 for 6 h, representative of $n = 4$. c-MYC target genes are separated into two groups: up-regulated c-MYC target genes and down-regulated c-MYC target genes. Mean fold change, standard deviation, and *p* value are provided for each target in Table S2. Respective quantifications are represented as means ± S.D. *, $p < 0.05$; **, $p < 0.01$; ***, $p < 0.001$; ****, $p < 0.0001$. *ns*, not significant.

MYC is overexpressed, activated, or stabilized in the cell. This is most likely because the negative regulation of MYC by PP2A is one of the more downstream events in MYC's "life cycle" and thus is not restricted to controlling only one component or step in the regulation of MYC stability. This is highlighted in the current work, because multiple models of MYC dependence

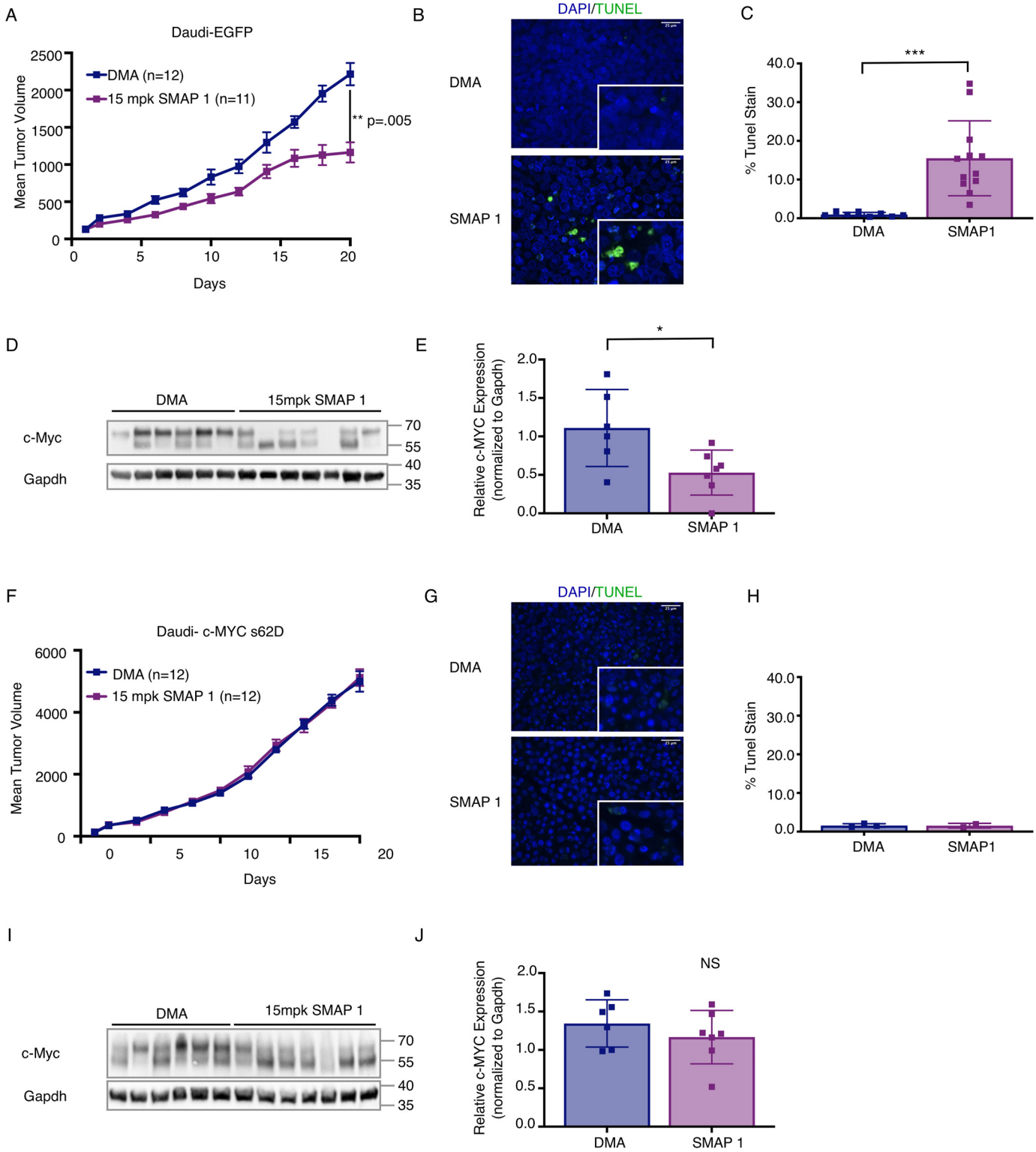

Figure 5. SMAP inhibition of tumor growth and changes to c-MYC expression is abrogated by mutation to c-MYC phosphodegron. *A*, tumor growth in a xenograft model of Daudi cell line expressing EGFP treated with DMA or SMAP1 twice a day. *B*, representative images of TUNEL staining in DMA- or SMAP1-treated Daudi–EGFP tumors. *C*, quantification of TUNEL in Daudi–EGFP tumors. *D*, Western blotting of untreated and treated tumor lysates for c-MYC in the Daudi–EGFP xenograft. *E*, quantification of c-MYC protein in DMA- and SMAP-treated Daudi–EGFP tumors in *D*, normalized to GAPDH. *F*, tumor growth in a xenograft model of Daudi cell line overexpressing c-MYC with a S62D mutation treated with DMA or SMAP1 twice a day. *G*, representative images of TUNEL staining in DMA- or SMAP1-treated tumors from the S62D xenograft. *H*, quantification of TUNEL in the S62D tumors. *I*, Western blotting of protein from tumor lysates for c-MYC from the S62D xenograft. *J*, quantification of c-MYC protein in DMA- and SMAP-treated tumors from the S62D xenograft in *I* normalized to GAPDH. Respective quantifications are represented as means ± S.D. *, $p < 0.05$; **, $p < 0.01$; ***, $p < 0.001$.

were tested including genetic amplification (Burkitt's lymphoma), post-translational stabilization (KRAS mutant cancers), and overexpression (TNBC).

Increased MYC expression is well-described to alter and regulate a number of cellular processes that cancer cells become addicted to including, but not limited to, cellular metabolism, cellular proliferation, cell survival, and differentiation (8). Future studies directed at understanding the processes that cells most depend upon in the context of increased MYC expression and PP2A dysregulation could help further define cancer subtypes most susceptible to this treatment strategy, as well as shed insight on potential resistance mechanisms to MYC-targeting strategies.

Additionally, although MYC is one of the better-characterized substrates of PP2A, PP2A has diverse cellular substrates. As demonstrated by our studies in KRAS mutant lung cancer models, we may be able to leverage our knowledge of defined PP2A substrates to identify disease contexts that are particularly susceptible to PP2A activation through coordinate effects of both MYC signaling and other oncogenic pathways including phosphatidylinositol 3-kinase and mitogen-activated protein kinase. Additionally, in triple-negative breast cancer, a MYC gene signature associated with activation has been proposed as a potential biomarker (74). Based on the research presented here, this subset of this particularly lethal disease may be especially treatment-sensitive to PP2A reactivation strategies.

Lastly, although the models presented here represent a variety of well-characterized examples of MYC-driven cancers, they represent only a subset of potential MYC targetable cancers. Specifically, this PP2A reactivation approach has the potential to be translated to multiple models of MYC-driven cancer such as pancreatic cancer, which is similar to NSCLC in the common co-expression of KRAS and MYC, as well as prostate cancer, in which MYC has been implicated in the deregulation of the AR-driven transcriptional programs and is associated with poor response to AR directed therapies. Indeed, it was recently published that SMAPs synergize with mammalian target of rapamycin inhibition in pancreatic cancer to reduce tumor growth through decreased MYC expression (50). Moreover, SMAPs were previously shown by our group to impact prostate cancer growth via destabilization of the androgen receptor, resulting in marked changes in its downstream transcriptional activity (47). Thus, this work could lay the foundation for the use of PP2A reactivation strategies in combination with AR-directed treatments to drive more durable treatment responses or as a single agent in enzalutamide-resistant metastatic prostate cancer. Overall, the work presented here expands the spectrum of cancer models in which PP2A activation is efficacious and suggests that therapeutic PP2A activation by SMAPs may be a useful strategy for the treatment of MYC-driven cancers.

Experimental procedures

Cell lines and reagents

Burkitt's lymphoma cell line Daudi, lung cancer cell line H441, and breast cancer cell lines MDA-MB-231, MDA-MB-453, SUM149PT, BT-549, and HCC1143 were purchased from the ATCC. H441 and Daudi cell lines were maintained in RPMI 1640 medium (Corning Mediatech, Inc., Manassas, VA). MDA-MB-231, MDA-MB-453, SUM149PT, BT-549, and HCC1143 were maintained in DMEM (Corning Mediatech, Inc., Manassas, VA). All media were supplemented with 10% fetal bovine serum (VWR International, Avantor Performance Materials, Center Valley, PA) and 50 units/ml of penicillin-streptomycin solution (GE Healthcare). The cells were maintained at 37 °C with 5% CO_2. Mycoplasma testing was performed routinely with a Lonza MycoAlert mycoplasma detection kit as per the manufacturer's protocol (catalog no. NC9922140; Thermo Fisher Scientific). SMAP compounds were diluted with DMSO to a stock concentration of 80 μM and stored at room temperature. Dilutions to the treatment concentrations were made in appropriate RPMI or DMEM accordingly. MG-132 (Calbiochem, San Diego, CA) was dissolved and aliquoted in DMSO at a concentration of 50 mM, stored at −80, and serially diluted to 10 μM in medium. Cycloheximide solution (100 mg/ml) was purchased from Millipore Sigma (C4859) and stored as per the manufacturer's instructions.

MTT assay

The cells were treated with the SMAPs (dissolved in DMSO) and screened for cell viability through the MTT assay using the MTT kit (Sigma–Aldrich).

Mammosphere assay

Breast cancer cells were plated on ultra-low attachment plates (Fisher) at 25,000 cells/well in 2 ml of mammosphere medium (B27, basic fibroblast growth factor (20 ng/ml), EGF (20 ng/ml), gentamycin (100 μg/ml), and amino acids in DMEM/F-12). The medium was replenished every 3 days. Starting at day 4, the cultures were treated for 24 h with the indicated doses of SMAP and then imaged and quantified.

Constructs and generation of recombinant cell lines

MSCV-N GFP was a gift from Karl Munger (Addgene plasmid no. 37855). MSCV h c-MYC IRES GFP was a gift from John Cleveland (Addgene plasmid no. 18119; MIG-MYC_S62D and MIG-MYC_T58A were generated from MSCV h c-MYC IRES GFP using the QuikChange Lightning site-directed mutagenesis kit (Agilent) according to the manufacturer's protocol using the primers 5′-ACCCCGCCCCTGGACCCTAGCCGCCG-3′ and 5′-CGGCGGCTAGGGTCCAGGGGCGGGGT-3′ (MIG-MYC_S62D) or 5-AGCTGCTGCCCGCCCCGCCCCTG-3′ and 5′-CAGGGGCGGGGCGGGCAGCAGCT-3′ (MIG-MYC_T58A). For retroviral transduction, Gryphon packaging cells (Allele Biotechnology) were transfected using X-tremeGENE HP (Roche) using a 2:1 ratio of transfection reagent to plasmid DNA. Transfection medium was replaced after 12 h. After 30 h, medium containing viral particles was collected and directly used to transduce H358 cells. The transduced cells were sorted for GFP positivity using a BD FACSAria, and MYC overexpression was confirmed by Western blotting. Daudi cells were transduced with viral supernatant in RetroNectin-coated 6-well plates (Takara Bio USA, Inc.) according to the manufacturer's protocol (RetroNectin-bound

virus infection method). Transduced cells were sorted for GFP as described for H358 cells.

Mouse models and treatment studies

$Kras^{LA2}$ mice were purchased from the National Cancer Institute Mouse Repository. For xenograft studies, 5×10^6 Daudi cells were injected subcutaneously into the right flank of 6–8-week-old female Nod-Scid mice in a 1:1 suspension of RPMI:Matrigel. 2.5×10^6 MDA-MB-231 or 1×10^6 SUM149PT cells were injected orthotopically into the right mammary fat pad of female NSG mice in a 1:1 suspension of DMEM and Matrigel. 5×10^6 MDA-MB-453 cells were injected subcutaneously into male NSG mice in a 1:1 suspension of DMEM and Matrigel. 5×10^6 of H441 cells were injected subcutaneously in the 6–8-week-old male nude mice (Strain 490, National Cancer Institute) in a 1:1 suspension of RPMI:Matrigel. The tumors were measured every other day by caliper, and body weight was measured every 4 days. The mice were treated with SMAPs or paclitaxel when average tumor volume reached ~100 mm^3. Daudi, MDA-MB-231, and H441 xenografts were treated until mice had a body conditioning score of 1, tumor volume exceeded 1200 mm^3, or the study reached 30 days, respectively. SUM149PT tumors were treated for 20 days, and MDA-MB-453 tumors were treated for 33 days. At termination of study, the mice received a final treatment 2 h before sacrifice. Tumor tissue was collected and formalin-fixed for IHC and snap-frozen in liquid nitrogen for immunoblotting and mRNA analysis.

In vivo administration of SMAPs

SMAPs were delivered by oral gavage, twice a day at 5 or 15 mg/kg in a solution of 10% *N*,*N*-dimethylacetamide (DMA) and 10% Solutol® HS15 (Kolliphor® HS 15) in sterile water.

In vivo administration of paclitaxel

20 mg/kg paclitaxel was delivered via intraperitoneal injection once per week. Paclitaxel was dissolved in DMSO followed by the addition of a prewarmed 1:1 solution of sterile water and propylene glycol such that the final DMSO concentration was 20%.

Antibodies and immunoblot analyses

The cells were washed twice in PBS upon collection and then lysed in radioimmune precipitation assay buffer (Thermo Fisher Scientific) containing phosphatase and protease inhibitors (Roche). Proteins lysates were separated by SDS-PAGE 12% polyacrylamide gels (Bio-Rad) and transferred to nitrocellulose membranes (Bio-Rad). The membranes were probed with anti–phospho-c-MYC s62 (Abcam), anti–phospho-c-MYC t58 (Abcam), total c-MYC (Cell Signaling), gapdh (Santa Cruz), and vinculin (Santa Cruz). Primary antibodies were probed with either goat anti-mouse (Abcam, Cambridge, UK) or donkey anti-rabbit (GE Healthcare) conjugated to horseradish peroxidase and imaged and quantified using the Bio-Rad ChemiDoc XRS chemiluminescence imager and software. All values were normalized to vinculin, gapdh, or total protein expression (using the Bio-Rad stain-free gels) and expressed as fold change relative to control.

Quantitative real-time quantitative PCR

Total RNA was extracted using the High Pure RNA isolation kit (Roche). cDNA synthesis was carried out using the iScript cDNA synthesis kit (Bio-Rad) as per the manufacturer's instructions. Sequences can be found in Table S1. Real-time PCR was performed with SYBR green PCR Master Mix (Applied Biosystems) on the Applied Biosystems 7900HT Fast Real-Time PCR System.

TUNEL staining

Tissue was fixed in 10% buffered formalin phosphate (Thermo Fisher Scientific; catalog no. SF100-4), transferred to 70% ethanol, and blocked in paraffin. Serial tissue sections (5 μm thick) were cut from the paraffin-embedded blocks and placed on charged glass slides. The ApopTag fluorescein *in situ* apoptosis detection kit (Millipore) was used according to the manufacturer's protocol to perform the TUNEL assay. Before the addition of terminal deoxynucleotidyl transferase enzyme, sections were deparaffinized with xylene and rehydrated through graded alcohol washes. VECTASHIELD mounting medium with propidium iodide (Vector Labs) was used for counterstaining in the $KRAS^{LA2}$ and H441 xenograft models. All other studies were counterstained for 4′,6′-diamino-2-phenylindole and mounted with ProLong™ Diamond Antifade Mountant (Molecular Probes catalog no. P36961) Fluorescent images were captured using the Zeiss Axioplan 2 IE microscope. Quantification was completed using the cell counter function of ImageJ. Imaging was performed at the Microscopy Cores at the Icahn School of Medicine at Mount Sinai and University of Michigan School of Medicine.

Immunohistochemistry

Tissue was fixed in 10% buffered formalin phosphate (Thermo Fisher Scientific; catalog no. SF100-4), transferred to 70% ethanol, and blocked in paraffin. Serial tissue sections (5 μm thick) were cut from the paraffin-embedded blocks and placed on charged glass slides. Tumor sections were stained with H&E and c-MYC (Abcam, ab32072). Briefly, sections were deparaffinized with xylene and rehydrated through graded alcohol washes followed by antigen retrieval in a pressure cooker (Dako) in citrate buffer (10 μM, pH 6.0, Vector Labs). The slides were then incubated in hydrogen peroxide/methanol, followed by incubation in normal goat serum in PBS. Antibody was applied overnight at 4 °C. DAB substrate was applied followed by counterstaining in hematoxylin. The images were captured with Olympus MVX10 (H&E) or Zeiss Axioplan 2IE (IHC) microscope. Imaging was performed at the Microscopy Core at the Icahn School of Medicine at Mount Sinai.

Statistics

Analysis was performed using GraphPad Prism 7. Statistical significance was assumed for a two-tailed p value of less than 0.05 using Student's t test or two-way analysis of variance with Tukey's post hoc test (presented as means; *error bars* indicate S.E. or S.D. as noted in the figures).

Study approval

Animal studies were performed under protocols approved by the Institutional Animal Care and Use Committee of the Center for Comparative Medicine and Surgery at the Icahn School of Medicine at Mount Sinai (protocol no. IACUC-2013-1426/ Novel Small Molecules to Treat Cancer), Case Western Reserve University (protocol nos. 2013-0130 and 2013-0132), and Oregon Health and Sciences University (protocol no. IP00001014).

Author contributions—C. C. F., E. Y., M. G., R. S., and G. N. conceptualization; C. C. F., E. Y., S. M., S. I., L. H., B. L. A.-P., M. J., E. C., G. W., and J. S. data curation; C. C. F., S. I., B. L. A.-P., M. J., and E. C. formal analysis; C. C. F., E. Y., S. M., L. H., and G. W. validation; C. C. F., E. Y., S. M., S. I., L. H., B. L. A.-P., M. J., and J. S. investigation; C. C. F. and J. S. visualization; C. C. F. methodology; C. C. F. writing-original draft; C. C. F., J. S., and G. N. project administration; C. C. F., E. Y., S. M., B. L. A.-P., M. G., R. S., J. S., and G. N. writing-review and editing; M. G., R. S., J. S., and G. N. supervision; M. G. and G. N. funding acquisition; G. N. resources.

Acknowledgments—We acknowledge the contributions of Shirish Shenolikar for insight and critical evaluation of the work. We also thank Caitlin O'Connor for assistance with the manuscript. We acknowledge the support of the Young Scientist Foundation.

References

1. Beroukhim, R., Mermel, C. H., Porter, D., Wei, G., Raychaudhuri, S., Donovan, J., Barretina, J., Boehm, J. S., Dobson, J., Urashima, M., Mc Henry, K. T., Pinchback, R. M., Ligon, A. H., Cho, Y. J., Haery, L., *et al.* (2010) The landscape of somatic copy-number alteration across human cancers. *Nature* **463,** 899–905 CrossRef Medline
2. Ohshima, K., Hatakeyama, K., Nagashima, T., Watanabe, Y., Kanto, K., Doi, Y., Ide, T., Shimoda, Y., Tanabe, T., Ohnami, S., Ohnami, S., Serizawa, M., Maruyama, K., Akiyama, Y., Urakami, K., *et al.* (2017) Integrated analysis of gene expression and copy number identified potential cancer driver genes with amplification-dependent overexpression in 1,454 solid tumors. *Sci. Rep.* **7,** 641 CrossRef Medline
3. Schaub, F. X., Dhankani, V., Berger, A. C., Trivedi, M., Richardson, A. B., Shaw, R., Zhao, W., Zhang, X., Ventura, A., Liu, Y., Ayer, D. E., Hurlin, P. J., Cherniack, A. D., Eisenman, R. N., Bernard, B., *et al.* (2018) Pan-cancer alterations of the MYC oncogene and its proximal network across the Cancer Genome Atlas. *Cell Systems* **6,** 282–300.e2 CrossRef Medline
4. Meyer, N., and Penn, L. Z. (2008) Reflecting on 25 years with MYC. *Nat. Rev. Cancer* **8,** 976–990 CrossRef Medline
5. Adhikary, S., and Eilers, M. (2005) Transcriptional regulation and transformation by Myc proteins. *Nat. Rev. Mol. Cell Biol.* **6,** 635–645 CrossRef Medline
6. Arvanitis, C., and Felsher, D. W. (2006) Conditional transgenic models define how MYC initiates and maintains tumorigenesis. *Semin. Cancer Biol.* **16,** 313–317 CrossRef Medline
7. Yeh, E., Cunningham, M., Arnold, H., Chasse, D., Monteith, T., Ivaldi, G., Hahn, W. C., Stukenberg, P. T., Shenolikar, S., Uchida, T., Counter, C. M., Nevins, J. R., Means, A. R., and Sears, R. (2004) A signalling pathway controlling c-Myc degradation that impacts oncogenic transformation of human cells. *Nat. Cell Biol.* **6,** 308–318 CrossRef Medline
8. Chen, H., Liu, H., and Qing, G. (2018) Targeting oncogenic Myc as a strategy for cancer treatment. *Signal Transduct. Target. Ther.* **3,** 5 CrossRef Medline
9. Soucek, L., Helmer-Citterich, M., Sacco, A., Jucker, R., Cesareni, G., and Nasi, S. (1998) Design and properties of a Myc derivative that efficiently homodimerizes. *Oncogene* **17,** 2463–2472 CrossRef Medline
10. Soucek, L., Jucker, R., Panacchia, L., Ricordy, R., Tatò, F., and Nasi, S. (2002) Omomyc, a potential Myc dominant negative, enhances Myc-induced apoptosis. *Cancer Res.* **62,** 3507–3510 Medline
11. Soucek, L., Nasi, S., and Evan, G. I. (2004) Omomyc expression in skin prevents Myc-induced papillomatosis. *Cell Death Differ.* **11,** 1038–1045 CrossRef Medline
12. Soucek, L., Whitfield, J. R., Sodir, N. M., Massó-Vallés, D., Serrano, E., Karnezis, A. N., Swigart, L. B., and Evan, G. I. (2013) Inhibition of Myc family proteins eradicates KRas-driven lung cancer in mice. *Genes Dev.* **27,** 504–513 CrossRef Medline
13. Savino, M., Annibali, D., Carucci, N., Favuzzi, E., Cole, M. D., Evan, G. I., Soucek, L., and Nasi, S. (2011) The action mechanism of the Myc inhibitor termed Omomyc may give clues on how to target Myc for cancer therapy. *PLoS One* **6,** e22284 CrossRef Medline
14. Jung, L. A., Gebhardt, A., Koelmel, W., Ade, C. P., Walz, S., Kuper, J., von Eyss, B., Letschert, S., Redel, C., d'Artista, L., Biankin, A., Zender, L., Sauer, M., Wolf, E., Evan, G., *et al.* (2017) OmoMYC blunts promoter invasion by oncogenic MYC to inhibit gene expression characteristic of MYC-dependent tumors. *Oncogene* **36,** 1911–1924 CrossRef Medline
15. Bandopadhayay, P., Bergthold, G., Nguyen, B., Schubert, S., Gholamin, S., Tang, Y., Bolin, S., Schumacher, S. E., Zeid, R., Masoud, S., Yu, F., Vue, N., Gibson, W. J., Paolella, B. R., Mitra, S. S., *et al.* (2014) BET bromodomain inhibition of MYC-amplified medulloblastoma. *Clin. Cancer Res.* **20,** 912–925 CrossRef Medline
16. Choi, S. K., Hong, S. H., Kim, H. S., Shin, C. Y., Nam, S. W., Choi, W. S., Han, J. W., and You, J. S. (2016) JQ1, an inhibitor of the epigenetic reader BRD4, suppresses the bidirectional MYC-AP4 axis via multiple mechanisms. *Oncol. Rep.* **35,** 1186–1194 CrossRef Medline
17. Delmore, J. E., Issa, G. C., Lemieux, M. E., Rahl, P. B., Shi, J., Jacobs, H. M., Kastritis, E., Gilpatrick, T., Paranal, R. M., Qi, J., Chesi, M., Schinzel, A. C., McKeown, M. R., Heffernan, T. P., Vakoc, C. R., *et al.* (2011) BET bromodomain inhibition as a therapeutic strategy to target c-Myc. *Cell* **146,** 904–917 CrossRef Medline
18. Ott, C. J., Kopp, N., Bird, L., Paranal, R. M., Qi, J., Bowman, T., Rodig, S. J., Kung, A. L., Bradner, J. E., and Weinstock, D. M. (2012) BET bromodomain inhibition targets both c-Myc and IL7R in high-risk acute lymphoblastic leukemia. *Blood* **120,** 2843–2852 CrossRef Medline
19. Tögel, L., Nightingale, R., Chueh, A. C., Jayachandran, A., Tran, H., Phesse, T., Wu, R., Sieber, O. M., Arango, D., Dhillon, A. S., Dawson, M. A., Diez-Dacal, B., Gahman, T. C., Filippakopoulos, P., Shiau, A. K., *et al.* (2016) Dual targeting of bromodomain and extraterminal domain proteins, and WNT or MAPK signaling, inhibits c-MYC expression and proliferation of colorectal cancer cells. *Mol. Cancer Ther.* **15,** 1217–1226 CrossRef Medline
20. Zhang, Z., Ma, P., Jing, Y., Yan, Y., Cai, M. C., Zhang, M., Zhang, S., Peng, H., Ji, Z. L., Di, W., Gu, Z., Gao, W. Q., and Zhuang, G. (2016) BET bromodomain inhibition as a therapeutic strategy in ovarian cancer by downregulating FoxM1. *Theranostics* **6,** 219–230 CrossRef Medline
21. Whitfield, J. R., Beaulieu, M. E., and Soucek, L. (2017) Strategies to inhibit Myc and their clinical applicability. *Front. Cell Dev. Biol.* **5,** 10 Medline
22. Allen-Petersen, B. L., and Sears, R. C. (2019) Mission possible: advances in MYC therapeutic targeting in cancer. *BioDrugs* **33,** 539–553 CrossRef Medline
23. Arroyo, J. D., and Hahn, W. C. (2005) Involvement of PP2A in viral and cellular transformation. *Oncogene* **24,** 7746–7755 CrossRef Medline
24. Chen, W., Arroyo, J. D., Timmons, J. C., Possemato, R., and Hahn, W. C. (2005) Cancer-associated PP2A Aα subunits induce functional haploinsufficiency and tumorigenicity. *Cancer Res.* **65,** 8183–8192 CrossRef Medline
25. Sablina, A. A., and Hahn, W. C. (2007) The role of PP2A A subunits in tumor suppression. *Cell Adhesion Migration* **1,** 140–141 CrossRef Medline
26. Janssens, V., and Goris, J. (2001) Protein phosphatase 2A: a highly regulated family of serine/threonine phosphatases implicated in cell growth and signalling. *Biochem. J.* **353,** 417–439 CrossRef Medline
27. Janssens, V., Goris, J., and Van Hoof, C. (2005) PP2A: the expected tumor suppressor. *Curr. Opin. Genet. Dev.* **15,** 34–41 CrossRef Medline
28. Lambrecht, C., Libbrecht, L., Sagaert, X., Pauwels, P., Hoorne, Y., Crowther, J., Louis, J. V., Sents, W., Sablina, A., and Janssens, V. (2018) Loss of protein phosphatase 2A regulatory subunit B56δ promotes spontaneous tumorigenesis *in vivo*. *Oncogene* **37,** 544–552 CrossRef Medline

29. Sents, W., Meeusen, B., Kalev, P., Radaelli, E., Sagaert, X., Miermans, E., Haesen, D., Lambrecht, C., Dewerchin, M., Carmeliet, P., Westermarck, J., Sablina, A., and Janssens, V. (2017) PP2A inactivation mediated by PPP2R4 haploinsufficiency promotes cancer development. *Cancer Res.* **77,** 6825–6837 CrossRef Medline
30. Arnold, H. K., and Sears, R. C. (2008) A tumor suppressor role for PP2A-B56α through negative regulation of c-Myc and other key oncoproteins. *Cancer Metastasis Rev.* **27,** 147–158 CrossRef Medline
31. Arnold, H. K., and Sears, R. C. (2006) Protein phosphatase 2A regulatory subunit B56α associates with c-myc and negatively regulates c-myc accumulation. *Mol. Cell Biol.* **26,** 2832–2844 CrossRef Medline
32. Sears, R. C. (2004) The life cycle of c-Myc: from synthesis to degradation. *Cell Cycle* **3,** 1133–1137 Medline
33. Escamilla-Powers, J. R., and Sears, R. C. (2007) A conserved pathway that controls c-Myc protein stability through opposing phosphorylation events occurs in yeast. *J. Biol. Chem.* **282,** 5432–5442 CrossRef Medline
34. Janghorban, M., Farrell, A. S., Allen-Petersen, B. L., Pelz, C., Daniel, C. J., Oddo, J., Langer, E. M., Christensen, D. J., and Sears, R. C. (2014) Targeting c-MYC by antagonizing PP2A inhibitors in breast cancer. *Proc. Natl. Acad. Sci. U.S.A.* **111,** 9157–9162 CrossRef Medline
35. Farrell, A. S., Allen-Petersen, B., Daniel, C. J., Wang, X., Wang, Z., Rodriguez, S., Impey, S., Oddo, J., Vitek, M. P., Lopez, C., Christensen, D. J., Sheppard, B., and Sears, R. C. (2014) Targeting inhibitors of the tumor suppressor PP2A for the treatment of pancreatic cancer. *Mol. Cancer Res.* **12,** 924–939 CrossRef Medline
36. Agarwal, A., MacKenzie, R. J., Pippa, R., Eide, C. A., Oddo, J., Tyner, J. W., Sears, R., Vitek, M. P., Odero, M. D., Christensen, D. J., and Druker, B. J. (2014) Antagonism of SET using OP449 enhances the efficacy of tyrosine kinase inhibitors and overcomes drug resistance in myeloid leukemia. *Clin. Cancer Res.* **20,** 2092–2103 CrossRef Medline
37. Arriazu, E., Pippa, R., and Odero, M. D. (2016) Protein phosphatase 2A as a therapeutic target in acute myeloid leukemia. *Front. Oncol.* **6,** 78 Medline
38. Hu, X., Garcia, C., Fazli, L., Gleave, M., Vitek, M. P., Jansen, M., Christensen, D., and Mulholland, D. J. (2015) Inhibition of Pten deficient castration resistant prostate cancer by targeting of the SET–PP2A signaling axis. *Sci. Rep.* **5,** 15182 CrossRef Medline
39. Neviani, P., and Perrotti, D. (2014) SETting OP449 into the PP2A-activating drug family. *Clin. Cancer Res.* **20,** 2026–2028 CrossRef Medline
40. O'Connor, C. M., Perl, A., Leonard, D., Sangodkar, J., and Narla, G. (2018) Therapeutic targeting of PP2A. *Int. J. Biochem. Cell Biol.* **96,** 182–193 CrossRef Medline
41. Pippa, R., Dominguez, A., Christensen, D. J., Moreno-Miralles, I., Blanco-Prieto, M. J., Vitek, M. P., and Odero, M. D. (2014) Effect of FTY720 on the SET-PP2A complex in acute myeloid leukemia: SET binding drugs have antagonistic activity. *Leukemia* **28,** 1915–1918 CrossRef Medline
42. Ramaswamy, K., Spitzer, B., and Kentsis, A. (2015) Therapeutic re-activation of protein phosphatase 2A in acute myeloid leukemia. *Front. Oncol.* **5,** 16 Medline
43. Richard, N. P., Pippa, R., Cleary, M. M., Puri, A., Tibbitts, D., Mahmood, S., Christensen, D. J., Jeng, S., McWeeney, S., Look, A. T., Chang, B. H., Tyner, J. W., Vitek, M. P., Odero, M. D., Sears, R., *et al.* (2016) Combined targeting of SET and tyrosine kinases provides an effective therapeutic approach in human T-cell acute lymphoblastic leukemia. *Oncotarget* **7,** 84214–84227 Medline
44. Sangodkar, J., Farrington, C. C., McClinch, K., Galsky, M. D., Kastrinsky, D. B., and Narla, G. (2016) All roads lead to PP2A: exploiting the therapeutic potential of this phosphatase. *FEBS J.* **283,** 1004–1024 CrossRef Medline
45. Kastrinsky, D. B., Sangodkar, J., Zaware, N., Izadmehr, S., Dhawan, N. S., Narla, G., and Ohlmeyer, M. (2015) Reengineered tricyclic anti-cancer agents. *Bioorg. Med. Chem.* **23,** 6528–6534 CrossRef Medline
46. Kauko, O., O'Connor, C. M., Kulesskiy, E., Sangodkar, J., Aakula, A., Izadmehr, S., Yetukuri, L., Yadav, B., Padzik, A., Laajala, T. D., Haapaniemi, P., Momeny, M., Varila, T., Ohlmeyer, M., Aittokallio, T., *et al.* (2018) PP2A inhibition is a druggable MEK inhibitor resistance mechanism in KRAS-mutant lung cancer cells. *Sci. Transla. Med.* **10,** eaaq1093 CrossRef Medline
47. McClinch, K., Avelar, R. A., Callejas, D., Izadmehr, S., Wiredja, D., Perl, A., Sangodkar, J., Kastrinsky, D. B., Schlatzer, D., Cooper, M., Kiselar, J., Stachnik, A., Yao, S., Hoon, D., McQuaid, D., *et al.* (2018) Small-molecule activators of protein phosphatase 2A for the treatment of castration-resistant prostate cancer. *Cancer Res.* **78,** 2065–2080 CrossRef Medline
48. Sangodkar, J., Perl, A., Tohme, R., Kiselar, J., Kastrinsky, D. B., Zaware, N., Izadmehr, S., Mazhar, S., Wiredja, D. D., O'Connor, C. M., Hoon, D., Dhawan, N. S., Schlatzer, D., Yao, S., Leonard, D., *et al.* (2017) Activation of tumor suppressor protein PP2A inhibits KRAS-driven tumor growth. *J. Clin. Invest.* **127,** 2081–2090 CrossRef Medline
49. Tohmé, R., Izadmehr, S., Gandhe, S., Tabaro, G., Vallabhaneni, S., Thomas, A., Vasireddi, N., Dhawan, N. S., Ma'ayan, A., Sharma, N., Galsky, M. D., Ohlmeyer, M., Sangodkar, J., and Narla, G. (2019) Direct activation of PP2A for the treatment of tyrosine kinase inhibitor-resistant lung adenocarcinoma. *JCI Insight* **4,** 125693 Medline
50. Allen-Petersen, B. L., Risom, T., Feng, Z., Wang, Z., Jenny, Z. P., Thoma, M. C., Pelz, K. R., Morton, J. P., Sansom, O. J., Lopez, C. D., Sheppard, B., Christensen, D. J., Ohlmeyer, M., Narla, G., and Sears, R. C. (2019) Activation of PP2A and inhibition of mTOR synergistically reduce MYC signaling and decrease tumor growth in pancreatic ductal adenocarcinoma. *Cancer Res.* **79,** 209–219 CrossRef Medline
51. Hummel, M., Bentink, S., Berger, H., Klapper, W., Wessendorf, S., Barth, T. F., Bernd, H. W., Cogliatti, S. B., Dierlamm, J., Feller, A. C., Hansmann, M. L., Haralambieva, E., Harder, L., Hasenclever, D., Kühn, M., *et al.* (2006) A biologic definition of Burkitt's lymphoma from transcriptional and genomic profiling. *N. Engl. J. Med.* **354,** 2419–2430 CrossRef Medline
52. Johnson, L., Mercer, K., Greenbaum, D., Bronson, R. T., Crowley, D., Tuveson, D. A., and Jacks, T. (2001) Somatic activation of the K-ras oncogene causes early onset lung cancer in mice. *Nature* **410,** 1111–1116 CrossRef Medline
53. Land, H., Parada, L. F., and Weinberg, R. A. (1983) Tumorigenic conversion of primary embryo fibroblasts requires at least two cooperating oncogenes. *Nature* **304,** 596–602 CrossRef Medline
54. Farrell, A. S., Joly, M. M., Allen-Petersen, B. L., Worth, P. J., Lanciault, C., Sauer, D., Link, J., Pelz, C., Heiser, L. M., Morton, J. P., Muthalagu, N., Hoffman, M. T., Manning, S. L., Pratt, E. D., Kendsersky, N. D., *et al.* (2017) MYC regulates ductal-neuroendocrine lineage plasticity in pancreatic ductal adenocarcinoma associated with poor outcome and chemoresistance. *Nat. Commun.* **8,** 1728 CrossRef Medline
55. Walz, S., Lorenzin, F., Morton, J., Wiese, K. E., von Eyss, B., Herold, S., Rycak, L., Dumay-Odelot, H., Karim, S., Bartkuhn, M., Roels, F., Wüstefeld, T., Fischer, M., Teichmann, M., Zender, L., *et al.* (2014) Activation and repression by oncogenic MYC shape tumour-specific gene expression profiles. *Nature* **511,** 483–487 CrossRef Medline
56. Richardson, G. E., and Johnson, B. E. (1993) The biology of lung cancer. *Semin. Oncol.* **20,** 105–127 Medline
57. Wolfer, A., Wittner, B. S., Irimia, D., Flavin, R. J., Lupien, M., Gunawardane, R. N., Meyer, C. A., Lightcap, E. S., Tamayo, P., Mesirov, J. P., Liu, X. S., Shioda, T., Toner, M., Loda, M., Brown, M., *et al.* (2010) MYC regulation of a "poor-prognosis" metastatic cancer cell state. *Proc. Natl. Acad. Sci. U.S.A.* **107,** 3698–3703 CrossRef Medline
58. Seo, A. N., Yang, J. M., Kim, H., Jheon, S., Kim, K., Lee, C. T., Jin, Y., Yun, S., Chung, J. H., and Paik, J. H. (2014) Clinicopathologic and prognostic significance of c-MYC copy number gain in lung adenocarcinomas. *Br. J. Cancer* **110,** 2688–2699 CrossRef Medline
59. Fukazawa, T., Maeda, Y., Matsuoka, J., Yamatsuji, T., Shigemitsu, K., Morita, I., Faiola, F., Durbin, M. L., Soucek, L., and Naomoto, Y. (2010) Inhibition of Myc effectively targets KRAS mutation-positive lung cancer expressing high levels of Myc. *Anticancer Res.* **30,** 4193–4200 Medline
60. Sears, R., Leone, G., DeGregori, J., and Nevins, J. R. (1999) Ras enhances Myc protein stability. *Mol. Cell* **3,** 169–179 CrossRef Medline
61. Sears, R., Nuckolls, F., Haura, E., Taya, Y., Tamai, K., and Nevins, J. R. (2000) Multiple Ras-dependent phosphorylation pathways regulate Myc protein stability. *Genes Dev.* **14,** 2501–2514 CrossRef Medline
62. Fallah, Y., Brundage, J., Allegakoen, P., and Shajahan-Haq, A. N. (2017) MYC-driven pathways in breast cancer subtypes. *Biomolecules* **7,** E53 Medline

63. Yang, A., Qin, S., Schulte, B. A., Ethier, S. P., Tew, K. D., and Wang, G. Y. (2017) MYC inhibition depletes cancer stem-like cells in triple-negative breast cancer. *Cancer Res.* **77,** 6641–6650 CrossRef Medline
64. Wang, E., Sorolla, A., Cunningham, P. T., Bogdawa, H. M., Beck, S., Golden, E., Dewhurst, R. E., Florez, L., Cruickshank, M. N., Hoffmann, K., Hopkins, R. M., Kim, J., Woo, A. J., Watt, P. M., and Blancafort, P. (2019) Tumor penetrating peptides inhibiting MYC as a potent targeted therapeutic strategy for triple-negative breast cancers. *Oncogene* **38,** 140–150 CrossRef Medline
65. Horiuchi, D., Kusdra, L., Huskey, N. E., Chandriani, S., Lenburg, M. E., Gonzalez-Angulo, A. M., Creasman, K. J., Bazarov, A. V., Smyth, J. W., Davis, S. E., Yaswen, P., Mills, G. B., Esserman, L. J., and Goga, A. (2012) MYC pathway activation in triple-negative breast cancer is synthetic lethal with CDK inhibition. *J. Exp. Med.* **209,** 679–696 CrossRef Medline
66. Lustig, L. C., Dingar, D., Tu, W. B., Lourenco, C., Kalkat, M., Inamoto, I., Ponzielli, R., Chan, W. C. W., Shin, J. A., and Penn, L. Z. (2017) Inhibiting MYC binding to the E-box DNA motif by ME47 decreases tumour xenograft growth. *Oncogene* **36,** 6830–6837 CrossRef Medline
67. Lee, J., Lim, B., Pearson, T., Choi, K., Fuson, J. A., Bartholomeusz, C., Paradiso, L. J., Myers, T., Tripathy, D., and Ueno, N. T. (2019) Anti-tumor and anti-metastasis efficacy of E6201, a MEK1 inhibitor, in preclinical models of triple-negative breast cancer. *Breast Cancer Res. Treat.* **175,** 339–351 CrossRef Medline
68. Nagaria, T. S., Shi, C., Leduc, C., Hoskin, V., Sikdar, S., Sangrar, W., and Greer, P. A. (2017) Combined targeting of Raf and Mek synergistically inhibits tumorigenesis in triple negative breast cancer model systems. *Oncotarget* **8,** 80804–80819 Medline
69. Giovannelli, P., Di Donato, M., Galasso, G., Di Zazzo, E., Bilancio, A., and Migliaccio, A. (2018) The androgen receptor in breast cancer. *Front. Endocrinol.* (*Lausanne*) **9,** 492 CrossRef Medline
70. Barfeld, S. J., Urbanucci, A., Itkonen, H. M., Fazli, L., Hicks, J. L., Thiede, B., Rennie, P. S., Yegnasubramanian, S., DeMarzo, A. M., and Mills, I. G. (2017) c-Myc antagonises the transcriptional activity of the androgen receptor in prostate cancer affecting key gene networks. *EBioMedicine* **18,** 83–93 CrossRef Medline
71. Sun, X. X., Sears, R. C., and Dai, M. S. (2015) Deubiquitinating c-Myc: USP36 steps up in the nucleolus. *Cell Cycle* **14,** 3786–3793 CrossRef Medline
72. Fernandez, P. C., Frank, S. R., Wang, L., Schroeder, M., Liu, S., Greene, J., Cocito, A., and Amati, B. (2003) Genomic targets of the human c-Myc protein. *Genes Dev.* **17,** 1115–1129 CrossRef Medline
73. Li, Z., Van Calcar, S., Qu, C., Cavenee, W. K., Zhang, M. Q., and Ren, B. (2003) A global transcriptional regulatory role for c-Myc in Burkitt's lymphoma cells. *Proc. Natl. Acad. Sci. U.S.A.* **100,** 8164–8169 CrossRef Medline
74. Qu, J., Zhao, X., Wang, J., Liu, X., Yan, Y., Liu, L., Cai, H., Qu, H., Lu, N., Sun, Y., Wang, F., Wang, J., and Zhang, J. (2017) MYC overexpression with its prognostic and clinicopathological significance in breast cancer. *Oncotarget* **8,** 93998–94008 Medline